Available online at www.sciencedirect.com

ScienceDirect

Procedia Computer Science 112 (2017) 1369–1377

Procedia Computer Science

www.elsevier.com/locate/procedia

International Conference on Knowledge Based and Intelligent Information and Engineering Systems, KES2017, 6-8 September 2017, Marseille, France

Feature definition, analysis and selection for cystoid region characterization in Optical Coherence Tomography

Joaquim de Moura[a], Plácido L. Vidal[a], Jorge Novo[a,*], José Rouco[a], Marcos Ortega[a]

[a] *University of A Coruña - Department of Computing, A Coruña (Spain)*

Abstract

Optical Coherence Tomography (OCT) is, nowadays, a clinical standard imaging technique in opthalmology as it provides more information than other classical modalities as can be, for instance, retinographies. OCT scans show a 3D representation of the real layout of the eye fundus in a non-invasive way, letting clinicians inspect deeply the retinal layers in a cross-sectional visualization. For that reason, OCT scans are commonly used in the study of the retinal morphology and the identification of pathological structures. Among them, an appropriate identification and analysis of any present intraretinal cystoid region is crucial to perform an adequate diagnosis of the exudative macular disease, one of the main causes of blindness in developed countries.

In this work, we analyzed and characterized the intraretinal cystoid regions in OCT images by the definition of a complete and heterogeneous set of 326 intensity and texture-based features. Relief-F and L0 feature selectors were used in order to identify the optimal feature subsets that provide the best discriminative power. Representative classifiers, as the Linear Bayes Normal Classifier (LDC), Quadratic Bayes Normal Classifier (QDC) and K-Nearest Neighbor Classifier (KNN) were finally used to evaluate the potential of identification of the feature subsets.

The method was validated using 51 OCT images. From them, 363 and 360 samples of cystoid and non-cystoid regions were selected, respectively. The best results were offered by the LDC classifier that, using a feature subset identified by the L0 selector, provided an accuracy of 0.9060.

Peer-review under responsibility of KES International

Keywords: Computer-aided diagnosis; retinal imaging, Optical Coherence Tomography, intraretinal cystoid region characterization, feature selection, classification

1. Introduction

Nowadays, retinal image analysis is a crucial task as a way for the diagnosis of different relevant diseases. In this context, an adequate identification of the relevant structures of the eye fundus as can be, for instance, the optic disc [1] or the arterio-venular vasculature [2], is crucial as they provide useful information for the characterization of cardiovascular diseases [3,4] or diabetes [5], among others. Over the years, different ophthalmological image modalities were presented, progressively improving the quality of the provided information. Among them, nowadays, Optical Coherence To-

* Jorge Novo. Faculty of Informatics. Campus de Elviña S/N, P.C. 15071 University of A Coruña. Tel.: +34-881016077 ; fax: +34-981167160.
E-mail address: joaquim.demoura@udc.es, placido.francisco.lizancos.vidal@udc.es, jnovo@udc.es, jrouco@udc.es, mortega@udc.es

1877-0509 © 2017 The Authors. Published by Elsevier B.V.
Peer-review under responsibility of KES International
10.1016/j.procs.2017.08.043

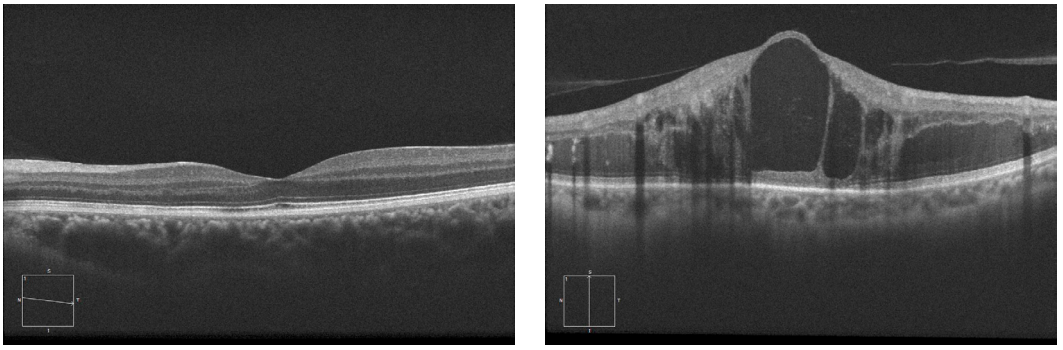

(a) (b)

Fig. 1. Examples of OCT sections. (a) OCT image without the presence of cysts. (b) OCT image with the presence of cysts.

mography (OCT) is widely used by experts as its capture consists of a non-invasive, contactless technique that offers a cross-sectional visualization of the eye fundus and its contained structures in a real time fashion[6]. This complete set of information outperforms other imaging modalities, as retinographies, since this higher detailed visualization of the retinal layers can help the specialists to achieve more accurate analysis of relevant pathologies as can represent the age-related macular degeneration (AMD)[7] or glaucoma[8].

Regarding AMD, this disease can derive in exudative macular disease that represents one of the main causes of blindness in developed countries. The intraretinal cystoid fluid is directly related with exudative macular disease, being originated by abnormal vasculature growing that may carry the leak of fluid. This fluid is progressively accumulated inside the retinal layers, deriving in a retinal architecture degeneration that damages the vision capability and carrying, in advanced stages, complete blindness. Fig. 1 shows a couple of representative examples of OCT images with and without the presence of cysts, respectively. Therefore, an early and precise identification of the presence of intraretinal cystoid regions and their characterization is crucial as it offers a suitable measurement of the disease severity, aiding clinicians in the development of more accurate diagnoses and treatments[9].

Over last years, some proposals arose that faced the task of cysts identification. The methods typically start with the identification of the retinal layers[10], as they delimit the region where the intraretinal cysts are placed. Posteriorly, most of the proposed methodologies aimed the cysts segmentation mainly by an initial detection of cysts candidates inside the retinal layers, followed by their analysis in terms of morphological and/or intensity properties in combination with post-processing stages that reduce the false positive (FP) rates preserving, therefore, the final cyst segmentation results. Following this strategy, Wilkins *et al.*[11] presented an automated technique that firstly applies a bilateral filter to reduce the typical speckle noise of the OCT images to facilitate the identification of the retinal layers. Then, this region is thresholded to obtain the aimed cyst segmentations. Post-processing rules are posteriorly applied to reduce the FP rate of the resultant segmentations. The work of Roychowdhury *et al.*[12] also begins with the identification of the retinal layers. In particular, the six main retinal layers are identified to posteriorly search for the dark regions among them. The candidates are finally analyzed using characteristics of solidity, mean and maximum intensities in order to identify the final cysts segmentations. González *et al.*[10] firstly applied watershed to the retinal layer region. Then, the obtained segmentations are grouped by connectivity and intensity-based similarity to produce the initial cyst candidates. As this strategy produces a large set of cyst candidates, the method posteriorly reduces the FPs using discarding rules in combination with a learning stage. Lang *et al.*[13] proposed a method for pixel classification, but its application was limited to the domain of micro-cystic identifications. Xu *et al.*[14] applied a layer-dependent stratified sampling to segment symptomatic exudate-associated derangements using voxel classification. Wang *et al.*[15] combined fuzzy C-Means with level sets to implement a methodology that combined the advantages of both strategies. Hence, the method is capable to identify fluid regions by intensity, provided by the fuzzy C-Means, and a suitable contour identification, produced by the level set method. In the case of Esmaeili *et al.*[16], the authors followed a thresholding strategy after a suitable speckle noise reduction using a K-SVD dictionary learning in curvelet transform that facilitates the segmentation process. As other cases, miss-extractions are finally filtered to produce the final segmentation results.

As we can see, most of the proposals designed methodologies that aimed the direct segmentation of the intraretinal cysts. This strategy presents a high dependency in the initial candidate segmentation stage as the application of inadequate segmentation techniques may produce large candidate sets, hardening the posterior FPs removal or forcing to apply strong reduction stages that may remove real extracted cysts. Moreover, imperfect cyst candidate segmentations can also induce to confusions in the posterior morphological/intensity analysis, penalizing the accuracy results.

Fig. 1 presents representative examples of regions that contain complex cyst segmentations. Many times, the fluid region contained by a cyst can be clearly observed inside the retinal layers. In this cases, the segmentation stage can produce acceptable results. However, other times, cysts do not present sufficient contrast to identify accurately their entire contour (Fig. 2(a) & (b)) or they appear in closed groups that make extremely complicated the identification of the limits of all of them (Fig. 2(c) & (d)).

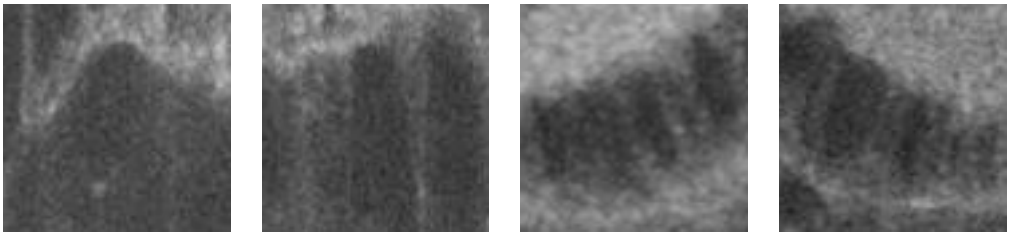

(a) (b) (c) (d)

Fig. 2. Examples of cysts. (a) & (b) Poorly defined cysts. (c) & (d) Closed groups of cysts.

This work faces the cyst identification process with a different strategy. Instead of classical candidate segmentation stages and posterior FP removal, we directly identify the intraretinal cystoid regions by the properties of the image. For that purpose, we analyzed the cystoid region properties and defined a large set of heterogeneous features that helped to characterize and identify the regions that contain cysts inside the retinal layers of an OCT scan. Subsets of features were selected in order to identify the ones that present the highest discriminative power. Finally, representative classifiers were used to evaluate the potential of the identified feature subsets.

2. Methodology

The system firstly identify the limits of the retinal layers, region where the intraretinal cystoid regions are contained. Posteriorly, windows of a defined size are analyzed and characterized by a complete set of features that help to identify those containing cysts.

2.1. Retinal layer segmentation

As cystoid regions are placed inside the retinal layers, the search space can be reduced by the identification of those layers in the OCT sections. In particular, the first intraretinal layer is the Inner Limiting Membrane (ILM) whereas the Retinal Pigment Epithelium (RPE) represents the bottom retinal layer, formed by pigmented cells at the external retinal region.

In this work, we used the methodology that was proposed by Chiu *et al.*[17]. This approach employs graph theory to represent the OCT sections as a graph of nodes. Dynamic programming is then used to extract the optimum connected paths from both sides of the OCT sections, paths that represent the limits of the visible layers. To that purpose, dark-to-light gradient images are obtained as they provide information of the limits of adjacent layers, normally being differentiated by contrast of intensities. These gradients represent scores and, therefore, the progressive minimum scored paths, found by the Dijkstra's algorithm[18], identify the searched main retinal layers. The original proposal was designed with the aim of identifying the main eight retinal layers. Despite that, we only identified the ILM and RPE layers as they represent the limits of the retinal layers, sufficient for the delimitation of the intraretinal cysts search space. In Fig. 3, an illustrative example of the ILM and RPE layer identification for a particular OCT image is shown.

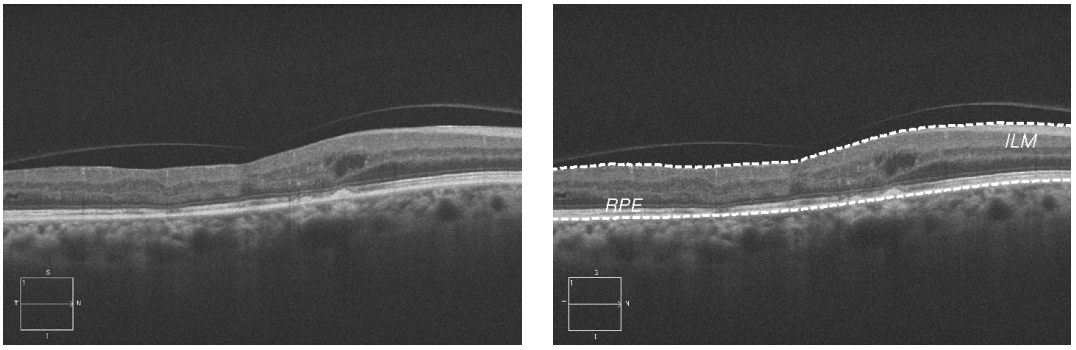

Fig. 3. Example of the segmentation of the ILM and RPE retinal layers.

2.2. Feature measurement

Each analyzed window inside the retinal layers is characterized by a complete and heterogeneous set of 326 features. Typically, the presence of cysts and their corresponding leak of fluid imply a depression of intensities in the cystoid region with respect to the surrounding neighbourhood, higher irregularity in the intensity profiles, larger inclusion of gradients as well as more heterogeneity in the gradient orientations, caused by the walls of the cysts. Based on that principles, we selected a set of 326 features providing a high potential in the discrimination power of the cystoid regions. Table 1 presents all the characteristics that were included in this work, herein described, organized by categories.

Global intensity-based features Using the intensities of the analyzed window, we measured the following features: *maximum, minimum, mean, median, standard deviation, variance,* 25^{th} *and* 75^{th} *percentile, skewness* and *maximum likelihood estimates for a normal distribution*.

GLIH Based on the concept that cystoid regions present a different histogram distribution, we measured different statistics over the histogram of the analyzed window: *obliquity, kurtosis, energy* and *entropy*.

Histogram of Oriented Gradients - HOG Normally, retinal layers present uniform shapes, with horizontal changes of intensities derived from the contiguous layers. Instead of that, cystoid regions present closed and/or oval shapes, with larger changes of intensities that imply bigger gradient sets and larger variability of orientations. These characteristics can be adequately captured by the HOG features[19] that can be suitable to characterize the gradient patterns in the analyzed windows. HOG presents invariance to scale, rotation or translation changes, useful strengths for an appropriate identification of cystoid regions of different sizes and locations inside the retinal layers. 9 windows combined with 9 histogram bins were extracted, summing a total of 81 HOG features.

Local Binary Patterns - LBP They[20] can be useful in the identification of patterns that normally appear with the normal layer tissue pattern or the presence of cysts. With a low complexity, they have also a low sensitivity to changes in illumination, important advantage that can be useful with the typical intensity variations that usually appear in the OCT scans due to changes in the configuration parameters and different capture machines. A wide range of parameters were studied, using a number of neighbors of 4, 8, 12 and 16 as well as a filter radius that varied from 1 to 8. This resulted in a total of 64 features that were analyzed.

Gabor filters Widely popular filters for texture analysis[21]. They can serve for capturing the texture of the fluid contained inside the cystoid regions as well as capturing the pattern of the normal retinal layer tissue. Gabor filters present, as main advantages, their invariance to rotation, translation or scale. They also present a remarkable robustness to deformations in the image, as intensity changes or the presence of noise, typical situations that normally appear in the analysis of OCT images. Two-dimensional Gabor filters are calculated over the

Table 1. Measured features. Other definitions: *max* - Maximum; *min* - Minimum; *std* - Standard Deviation

Category	**Features**
Global Intensity-Based Features - GIBS	[1-8] Max, min, mean, median, std, variance, percentiles 25 & 75 [9] skewness [10-13] maximum likelihood estimates
Gray-level Intensity Histogram - GLIH	[14-18] Obliquity, kurtosis, energy, entropy, mean intensity (μ)
Histogram of Oriented Gradients - HOG	[19-99] 9 windows per bound box & 9 histogram bins
Gabor filters	Orientations= 8 Scale= 5 & 8 [100-259] Mean and std
Local Binary Patterns - LBP	Number of neighbors= (4,8,12,16) Filter radius: 1-8 [260-323] Mean and std
Fractal dimension	[324-326] Mean, std, lacunarity

gray-level image[22] as a Gaussian kernel function modulated by a complex sinusoidal plane wave, represented by:

$$G(x,y) = \frac{f^2}{\pi\gamma\eta} exp\left(-\frac{x'^2 + \gamma^2 y'^2}{2\sigma^2}\right) exp\left(j2\pi f x' + \phi\right) \tag{1}$$

where f represents the frequency of the sinusoid, θ measures the orientation of the normal to the parallel stripes of a Gabor function, ϕ is the phase offset, σ indicates the standard deviation of the Gaussian envelope and γ is the spatial aspect ratio which specifies the ellipticity of the support of the Gabor function, where x' and y' are represented by:

$$\begin{aligned} x' &= xcos\theta + ysin\theta \\ y' &= -xsin\theta + ycos\theta \end{aligned} \tag{2}$$

In our case, two different banks of filters were set, one with 5 scales of frequencies, f, and another with 8. Both analyzed the same number of orientations θ, 8. General statistics are finally derived from the feature vectors to obtain 160 Gabor features.

Fractal dimension These features[23] transform the intensity of the analyzed window to the fractal dimension (FD) domain with the purpose of texture analysis of the fractal properties. These features, that already demonstrated their suitability in other medical imaging applications, are useful to capture texture information that otherwise

would be hidden. The intensity window transformation to FD domain is achieved with the differential box-counting (DBC) algorithm[24]. With the transformed FD image, we extract general statistics, the mean and the standard deviation as well as the lacunarity that measures the "lumpiness" of the fractal information.

2.3. Feature Selection and classification

Feature selection was applied to the entire feature set in order to obtain the most useful ones. This way, we preserve the features that provide the higher discriminative power avoiding, therefore, redundancies and fastening the cystoid region identification process. Two representative feature selector strategies, Relief-F and L0, were applied in a 10-fold cross validation process. Relief-F[25] samples instances randomly and checks the distance between them and the neighbours that have the same or different classes. A weight function uses the distances to, finally, rank them. L0[26] implies a simple optimization technique, using an adapted SVM, for minimizing the zero-norm of the weight vector that is represented by the feature set.

Regarding the classification stage, we selected three representative classifiers to test the suitability of the extracted features in the identification of the cystoid regions. We used the following: Linear Bayes Normal Classifier (LDC), Quadratic Bayes Normal Classifier (QDC) and K-Nearest Neighbor Classifier (KNN) with $k = 5$, value that was empirically established.

3. Results and discussion

The methodology was tested using 51 OCT histological images. The images were acquired with a confocal scanning laser ophtalmoscope, a CIRRUS^{TM}HD-OCT-Carl Zeiss Meditec. The images were acquired centered in the macula, from different patients and taken from both left and right eyes. Regarding the image resolution, a variability is represented including images from 924×616 to 1280×853. Different intensity and contrast configurations were also represented in the image dataset. The image dataset was used directly, without any preprocessing stage.

The image dataset was labeled by an expert clinician, identifying all the cysts that appear in the images. Using this groundtruth as reference a sample dataset was built, including 363 and 360 windows with and without the presence of cysts, respectively, summing a total of 723 samples. A window size of 51×51 was selected, taking a size large enough to include sufficient information of large cysts but not too much in order to avoid losing detection detail. The classification stage was performed by 10-fold cross-validation with 50 repetitions, being the mean error/accuracy calculated to measure the final performance of the method.

Regarding feature selection, we tested both analyzed strategies, Relief-F and L0, with the entire feature set to identify the most suitable feature subsets. Fig. 4 shows the error of the classification stage using the LDC and the KNN classifiers (QDC is similar to the LDC case) using progressive larger feature sets that were extracted with both selector strategies. In the case of the LDC, the L0 feature selector offered the best results whereas using the KNN both selectors offer similar results in large feature subsets. We analyzed until a maximum of 50 features because, as Fig. 4 shows, the error is stabilized.

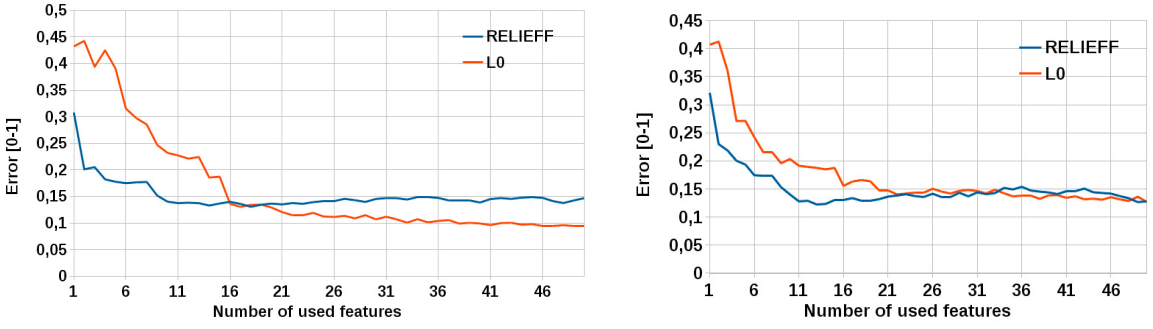

Fig. 4. Evolution of the error using the LDC classifier and progressive larger feature subsets provided by each feature selector method.

Table 2. Best accuracy obtained by each tested classifier and the feature selected sets by each method.

Method/Classifier	LDC	QDC	KNN(k = 5)
Relief-F	0.86968	0.86974	0.87759
L0	0.90598	0.88746	0.87305

Fig. 5 shows the selected features that were provided by each selector, of a total of 50, grouped by categories. As we can observe, HOG features were frequently selected as the orientation of the gradients is more uniform and repeated in the case of normal retinal tissue, being more distributed in the cases of the gradients caused by the cysts. Regarding the identification of the normal retinal layer and cystoid fluid tissues, each selector preferred one texture-based type: Gabor filters in the case of Relief-F and LBP in the case of L0. We would also like to highlight that despite that few global intensity-based features were defined, they were significantly selected by both strategies indicating the significant differentiation in the global intensity profiles of both types of regions.

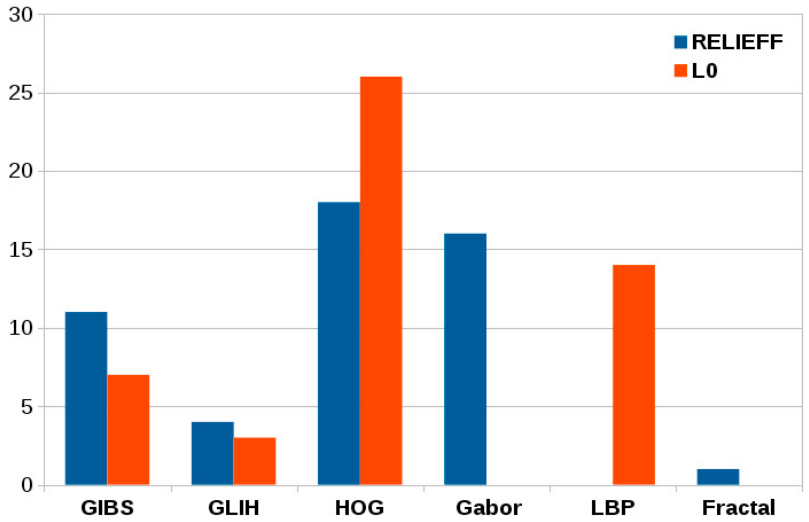

Fig. 5. Number of selected features, of a total of 50, by categories using each feature selector method.

Table 2 presents the best results of the classification stage that were achieved using different configurations and the selected features by each analyzed feature selector. As we can see, the worst results were offered by the LDC and QDC classifiers using feature subsets extracted with the Relief-F strategy whereas the best result was also provided by the LDC classifier but using a feature subset obtained with the L0 strategy, in this case.

Fig. 6 presents different examples of complex cystoid and non-cystoid regions that were correctly identified, demonstrating the robustness of the system. Fig. 6(a) shows a typical situation of a region that includes the projection zone of a vessel, implying an intensity drop that could be confused with the fluid tissue of a cyst. The case of Fig. 6(b) presents an irregular region derived of the presence of exudates that alters the retinal layers. In both cases, the system was capable to distinguish these irregularities as non-cystoid regions. Figs. 6(c) & (d) also show a couple of complex cystoid cases. The first one represents the typical case of a large cyst with a not very clear contour that the system was capable to identify. The second case shows a huge cyst significantly larger than the analyzed window size. In this case, we can see that the window belong to a fluid region inside a cyst.

Fig. 7 also shows representative miss-classifications. Sometimes, tiny cysts can be omitted by the system as they offer poor information for being identified (Fig. 7(a)). Moreover, in other cases, the combination of partial cysts with other structures, as exudates, can confuse the system, as the case of Fig. 7(b). Regarding non-cystoid regions, despite that most of the projected shadows are correctly identified as non-cystoid regions, close groups of shadows that appear in the analyzed regions, the system can understand this variability as cyst presence, as happened with Fig. 7(c). Other cases of retinal layer alterations that could not be directly implied as cyst presence can also be confused as a cyst presence (Fig. 7(d)).

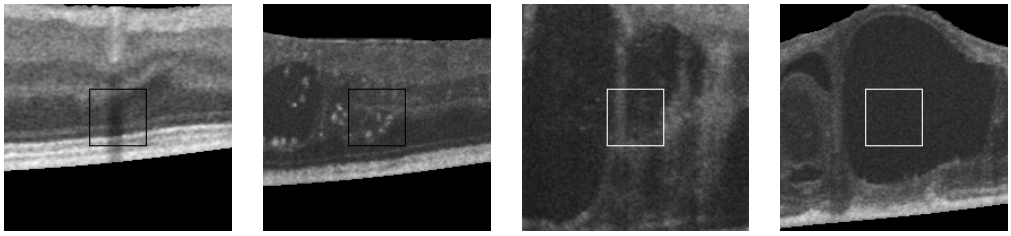

(a) (b) (c) (d)

Fig. 6. Examples of regions correctly classified. (a) & (b) Non-cystoid regions. (c) & (d) Cystoid regions.

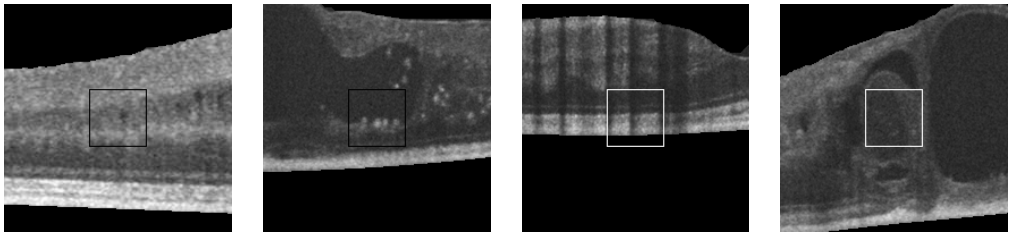

(a) (b) (c) (d)

Fig. 7. Examples of regions incorrectly classified. (a) & (b) Cystoid regions classified as non-cystoid. (c) & (d) Non-cystoid regions classified as cystoid.

4. Conclusions

The identification of cysts in OCT images is a crucial task for the analysis of relevant pathologies as is the exudative macular disease, one of the main causes of blindness in developed countries.

Instead of individual cyst segmentations that are faced by most of the proposed approaches, we faced this issue with an analysis by regions. This way, we identify and characterize any present intraretinal cystoid region inside the retinal layers as a way for the diagnosis of the exudative macular disease. We analyzed the main characteristics of these regions and their main differences with respect to the typical retinal layer tissue. As a result of this analysis, a complete and heterogeneous set of 326 intensity and texture-based features were implemented with the potential of discrimination of both cystoid and non-cystoid retinal regions. Representative feature selectors, as Relief-F and L0, were applied to the entire feature set to identify those ones that offer the best discriminative power, avoiding redundancies in the feature definition and facilitating the classification process. LDC, QDC and KNN classifiers were applied to the selected feature subsets in order to measure the performance of the system. Satisfactory results were obtained in the tests, achieving an accuracy of 0.9060 with the LDC classifier using a feature subset identified by the L0 selector.

As future work, a further analysis is planned to identify more suitable characteristics that can contribute to the identification of the cystoid regions. Moreover, wrapped-based feature selection methods will be tested as well as further classifiers. Regarding the validation stage, larger datasets are planned to be collected and tested in order to reinforce the conclusions achieved in this work.

Acknowledgements

This work is supported by the Instituto de Salud Carlos III, Government of Spain and FEDER funds of the European Union through the PI14/02161 and the DTS15/00153 research projects and by the Ministerio de Economía y Competitividad, Government of Spain through the DPI2015-69948-R research project.

References

1. Novo, J., Penedo, M., Santos, J.. Optic disc segmentation by means of GA-Optimized Topological Active Nets. *Lecture Notes in Computer Science: Image Analysis and Recognition, ICIAR'08* 2008;**5112**:807–816.

2. de Moura, J., Novo, J., Ortega, M., Charlón, P.. 3D retinal vessel tree segmentation and reconstruction with OCT images. *Lecture Notes in Computer Science: Image Analysis and Recognition, ICIAR'16* 2016;**9730**:807–816.
3. Wong, T., Klein, R., Sharrett, A., Duncan, B., Couper, D., Klein, B., et al. Retinal arteriolar diameters and elevated blood pressure: the atherosclerosis risk in communities study. *Annals of Internal Medicine* 2004;**140**:248–255.
4. Ikram M.K., d.J.F., Bos, M., Vingerling, J., Hofman, A., Koudstaal, P., de Jong, P., et al. Retinal vessel diameters and risk of stroke: the rotterdam study. *Neurology* 2006;**66**(9):1339–1343.
5. Wong, T., Klein, R., Sharrett, A., Schmidt, M., Pankow, J., Couper, D., et al. Retinal arteriolar narrowing and risk of diabetes mellitus in middle-aged persons. *Journal of the American Medical Association* 2002;**287**:2528–2533.
6. Puzyeyeva, O., Lam, W., Flanagan, J., Brent, M., Devenyi, R., Mandelcorn, M., et al. High-resolution optical coherence tomography retinal imaging: A case series illustrating potential and limitations. *Journal of Ophthalmology* 2011;.
7. Keane, P., Patel, P., Liakopoulos, S., Heussen, F., Sadda, S., Tufail, A.. Evaluation of age-related macular degeneration with optical coherence tomography. *Survey of Ophthalmology* 2012;**57**(5):389–414.
8. Geitzenauer, W., Hitzenberger, C., Schmidt-Erfurth, U.. Retinal optical coherence tomography: past, present and future perspectives. *British Journal of Ophthalmology* 2011;**95**(2):171–177.
9. Bogunovic, H., Abramoff, M., Zhang, L., Sonka, M.. Prediction of treatment response from retinal oct in patients with exudative age-related macular degeneration. *Ophth Med Image Analysis Workshop, MICCAI'14* 2014;:129–136.
10. González, A., Penedo, M., Vzquez, S., Novo, J., Charlón, P.. Cost function selection for a graph-based segmentation in OCT retinal images. *Computer Aided Systems Theory - EUROCAST 2013* 2013;**8112**:125–132.
11. Wilkins, G., Houghton, O., Oldenburg, A.. Automated segmentation of intraretinal cystoid fluid in optical coherence tomography. *IEEE Transactions on Biomedical Engineering* 2012;**59**(4):1109–1114.
12. Roychowdhury, S., Koozekanani, D., Radwan, S., Parhi, K.. Automated localization of cysts in diabetic macular edema using optical coherence tomography images. *International Conference of the IEEE Engineering in Medicine and Biology Society* 2013;:1426–1429.
13. Lang, A., Carass, A., Swingle, E., Al-Louzi, O., Bhargava, P., Saidha, S., et al. Automatic segmentation of microcystic macular edema in OCT. *Biomedical Optic Express* 2014;**6**(1):155–169.
14. Xu, X., Lee, K., Zhang, L., Sonka, M., Abràmoff, M.. Stratified sampling voxel classification for segmentation of intraretinal and subretinal fluid in longitudinal clinical OCT data. *IEEE Transactions on Medical Imaging* 2015;**34**(7):1616–1623.
15. Wang, J., Zhang, M., Pechauer, A., Liu, L., Hwang, T., Wilson D.J. Li, D., et al. Automated volumetric segmentation of retinal fluid on optical coherence tomography. *Biomedical Optic Express* 2016;**7**(4):1577–1589.
16. Esmaeili, M., Dehnavi, A., Rabbani, H., Hajizadeh, F.. Three-dimensional segmentation of retinal cysts from spectral-domain optical coherence tomography images by the use of three-dimensional curvelet based K-SVD. *Journal of Medical Signals and Sensors* 2016; **6**(3):166–171.
17. Chiu, S., Li, X., Nicholas, P., Toth, C., Izatt, J., Farsiu, S.. Automatic segmentation of seven retinal layers in SDOCT images congruent with expert manual segmentation. *Optics Express* 2010;**10**(10):19413–19428.
18. Dijkstra, E.. A note on two problems in connexion with graphs. *Numerische Mathematik* 1959;**1**(1):269–271.
19. Dalal, N., Triggs, B.. Histograms of oriented gradients for human detection. *Computer Vision and Pattern Recognition, CVPR'05* 2005; :886–893.
20. Ojala, T., Pietikainen, M., Maenpaa, T.. Multiresolution gray-scale and rotation invariant texture classification with local binary patterns. *IEEE Transactions on Pattern Analysis and Machine Intelligence* 2002;**24**(7):971–971.
21. Gabor, D.. Theory of communication. *J Institute of Electrical Engineering* 1946;**93**:429–457.
22. Haghighata, M., Zonouzb, S., Abdel-Mottaleba, M.. Cloudid: Trustworthy cloud-based and cross-enterprise biometric identification. *Expert Systems with Applications* 2015;**42**(21):7905–7916.
23. Al-Kadi, O., Watson, D.. Texture analysis of aggressive and nonaggressive lung tumor ce ct images. *IEEE Transactions on Biomedical Engineering* 2008;**55**(7):1822–1830.
24. Buczkowski, S., Kyriacos, S., Nekka, F., Cartilier, L.. The modified box-counting method: Analysis of some characteristic parameters. *Pattern Recognition* 1998;**31**:411–418.
25. Kononenko, I.. Estimating attributes: analysis and extensions of relief. In: *Machine Learning: ECML-94*. Springer; 1994, p. 171–182.
26. Weston, J., Elisseeff, A., Schölkopf, B., Tipping, M.. Use of the zero norm with linear models and kernel methods. *The Journal of Machine Learning Research* 2003;**3**:1439–1461.